FYP

Donovan Webb

Department of Physics, University of Bath, Bath BA2 7AY, United Kingdom

E-mail: `dw711@bath.ac.uk`

Abstract.

XXPREVIOUSXX A device capable of uniformly concentrating a magnetic fields inside of a free space cavity will increase the efficiency of many magnetic devices and sensors. This project shall look at a proposed design for a magnetic field concentrator informed by the transformation optic technique. A metamaterial shell comprised of high and low permeability sections alternating in the angular direction has been shown to approximate the designed concentrator[?]. The ability of the shell acting as a concentrator will be explored in various regimes with a specific focus on improving efficiency of wireless power transmission.

1. Introduction

The manipulation of magnetic fields is a critical tool for many modern technologies. Magnetic devices often have efficiencies dependent on the strength of interaction with an external magnetic field. Examples include energy harvesting from magnetic fields [?] to brain activity scans by locating small magnetic gradients [?]. These devices may have increased efficiency by concentrating the desired magnetic field within the area of sensing or harvesting.

Magnetic fields may be described by Maxwell's equations [?] and are guided by materials due to their optical properties, such as permitivity and permeability [?]. Fermat's principle of least time allowed the design of many optical devices using geometrical lenses [?], however, with the maturation of fabrication techniques, many materials may be produced with exotic anisotropic optical properties [?] prompting the development of transformation optics (TO) — a modern approach to optical device design.

Here we describe one such TO designed device; The magnetic concentrator [?], with a particular focus on its efficacy in wireless power transmission.

1.1. *Transformation Optics and Metamaterials*

TO informed the design of many new devices such as perfect lenses [], magenetic-hoses [], -cloaks [], -rotators [], -blackholes [], and -concentrators []. It can be shown that due to the form invariance of Maxwell's equations, a spatial coordinate transform is equivalent to the insertion of a material with specific permeabilities and permitivities. This is shown conceptually by the three steps of the schematic shown in figure 1. First a ray is considered in free cartesian space in panel a, which due to Fermat's principle of least time will be following the horizontal spatial grid lines. The space is then transformed arbitrarily in panel b so that the ray adopts the desired path for the final device. The transformation required, A, to morph the ray now informs the optical properties for the specific inserted material of panel c, which is once again located in untransformed space.

The form invariance of Faraday's law is described by the equivalent expressions

$$\nabla' \times \mathbf{E'} = -jw[\mu_0]\mathbf{H'} \qquad \textit{and} \qquad \nabla \times \mathbf{E} = -jw[\mu']\mathbf{H}, \tag{1}$$

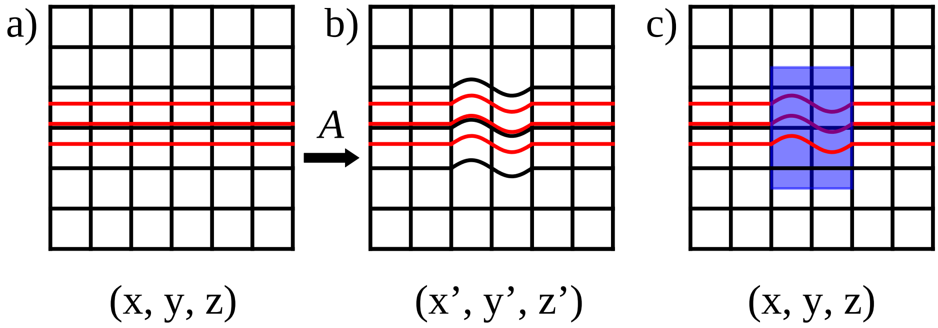

Figure 1. The steps of Transformation Optics. a) A ray (red) travelling in untransformed spatial coordinates (black grid) follows the path of least time. b) A spatial coordinate transformation A is applied to guide the ray along a desired path. c) A material (blue) is insterted into the untransformed space with corresponding permeability and permitivity which mimics the spatial coordinate transform A for the ray.

where the first is expressed in transformed coordinate space $x'(x,y,z), y'(x,y,z), z'(x,y,z)$ and free space permeability $[\mu_0]$, whilst the second is expressed in untransformed cartesian space x, y, z but with some space dependent permeability $[\mu']$. Equivalent expressions exist for the remaining Maxwell equations and similarly some non-free permittivity $[\epsilon']$ is required. The space dependant permeabilities and permittivities are found by,

$$\mu' = \frac{A\mu_0 A^T}{|A|} \qquad and \qquad \epsilon' = \frac{A\epsilon_0 A^T}{|A|} \tag{2}$$

where A is the Jacobian matrix describing the transformation of coordinate systems (e.g. between panel a and panel b in figure 1).
The resulting calculated optical properties may be anisotropic, have arbitrary magnitude and even be negative []. As bulk materials rarely, if ever, show these properties, optical metamaterials are often required [**?**].
Metamaterials are often comprised of repeating units whose dimensions are much smaller than the wavelength of the interacting radiation [**?**]. The individual units may have specific geometery, orientation and optical properties to selectively interact with incident waves so that the net effect of the material mimics a bulk substance with different optical properties than its substituent parts.

1.2. Magnetic Concentrator

As described above, a device capable of magnetic field concentration can increase the efficiency of sensors and energy harvesters. Utilising TO we may design an optimal field concentrator which fulfils the criteria: The magnetic field within a region A is concentrated into a cavity B where B is free space only. A possible geometry for this device that has cylindrical symmetry is shown on LHS of figure 2. To satisy these conditions two coordinate transforms are applied: First the region $\rho < R_2 - \eta$ is radially and linearly compressed to the region $\rho < R_1$; Second, to ensure the continuity of our transformed space, a high (k^{th}) order polynomial radial expansion of $R_2 - \eta < \rho < R_2$ to the region $R_1 < \rho < R_2$ is made. These transformations are described by the coordinate transformations,

$$\begin{aligned} \rho' &= \frac{R_1}{R_2 - \xi}\rho, \qquad & \rho' \in [0,\ R_2 - \xi) \\ \rho' &= R_2^{1-k}\rho^k \qquad & \rho' \in [R_2 - \xi,\ R_2). \end{aligned} \tag{3}$$

By symmetry we see that θ and z remain unchanged through the two transformations. The corresponding Jacobians may be found for these transformations and using equation 2, the permeabilities of the required inserted material may be found to be

$$
\begin{aligned}
\mu' &= \begin{pmatrix} 1 & 0 & 0 \\ 0 & 1 & 0 \\ 0 & 0 & (\frac{R_2-\xi}{R_1})^2 \end{pmatrix} & \rho' \in [0,\ R_1) \\
\mu' &= \begin{pmatrix} k & 0 & 0 \\ 0 & 1/k & 0 \\ 0 & 0 & \frac{1}{k}(\frac{\rho'}{R_2})^{2/k-2} \end{pmatrix} & \rho' \in [R_1,\ R_2)
\end{aligned}
\tag{4}
$$

Taking the limit $\eta \to 0$ in order to concentrate all of the field within A into B, and matching the boundary conditions at $R_2 - \eta$ and at $R1$, we find that $k \to \infty$. From this we find that the required permeability within B is satisfied by free space whilst a material with radial permeability $\mu_\rho \to \infty$ and angular permeability $\mu_\theta \to 0$ is required for region A. The z components of permeability are ignored as we assume the cyclindrical shell is infinitely long so the z component must be invariant. A model for this theoretical shell can be seen guiding an external magnetic field in the COMSOL simulation (figure 6 a).

To satisfy these highly anisotropic conditions practically, an exploration of metamaterials is required. A possible discretized shell construction is proposed [**?**] where the high radial permeability is provided by ferromagnetic materials whilst the angular permeability is shielded by superconducting material. Materials such as MuMetal, have relative permeabilities of up to $300,000+$ [**?**] and ideal superconductors in their Meissner state will exclude all magenetic fields from within their interior giving a relative permeability of 0 [**?**]. In an alternating field, a far cheaper option for blocking the angular magnetic field component is the use of copper sheeting. From Lenz's law an oscillating magnetic field perpendicular to a metal sheet will induce Eddy currents which will oppose the changing field. At an appropriate frequency, which is proportional to the copper thickness, the effective angular permeability is reduced to near zero. To approximate the conditions proposed by TO design, these two materials may be arranged in alternating angular sheets, as seen in figure 4.

In an external static uniform magnetic field, the ideal shell will increase the field within region B by a factor of R_2/R_1. Similarly if a magnetic dipole is surrounded by the concentrating shell, then the field outside of the shell will be increased by a factor of R_2/R_1.

1.3. Wireless Power Transfer

The ability to transfer power between devices that are not connected by wires is useful in many settings: for convenince, e.g. mobile phones; for safety, e.g. implanted medical devices; or for practicallity, e.g. satellites. We shall focus on near field power transmission by the use of inductive coupling. Inductive coupling transfers power between two coils of wire (two inductors) by an oscillating magnetic field. The transmitting coil is supplied with an alternating current, which by Ampere's law creates an oscillating magnetic field. The receiving coil is placed within this magnetic field so that a current is induced as described by Faraday's law. A schematic of these two coupled circuits can be seen in figure 3 a, b, and d. This strategy for power transfer is highly sensitive to distance as the magnetic field of a dipole drops off with distance cubed, r^{-3}, therefore the power is proportional to r^{-6} if the dipole is driven at a fixed frequency and current. The power transfer efficiency, PTE, also suffers with distance as the non-ideal resistive losses in the primary coil remain (relatively) constant with distance. To somewhat counteract this sharp drop off of efficiency with distance, concentrating shells may be used to magnify the transmitted field and locally concentrate the field around the receiving solenoid. The concentrating shell is larger than the coil by necessity, however the presence of a shell is always advantageous when the free space distance between the power transmitting and power receiving device is greater than k, where

$$k = \frac{R_2}{\sqrt[3]{R} - 1} \tag{5}$$

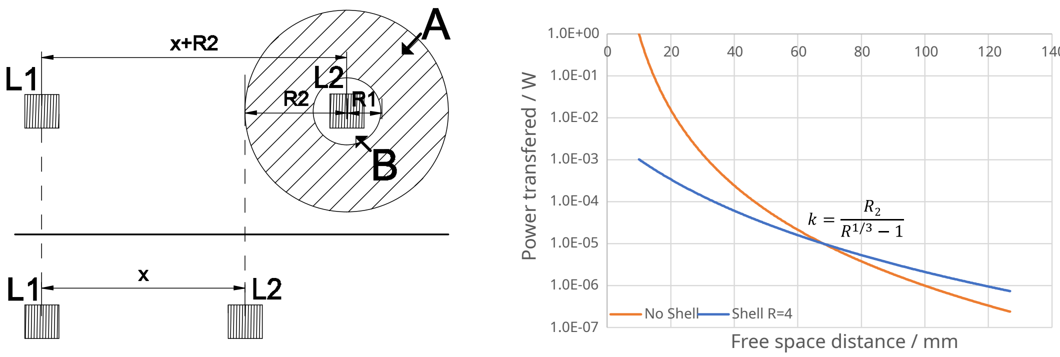

Figure 2. A concentrating shell with inner radius R_1 and outer radius R_2 is useful for increasing the efficiency of wireless power transmission by inductive coupling. PTE is highly sensitive to distance between coils being proportional to r^{-6}. A concentrating shell increases this power transfer by $(R_2/R_1)^2$ but at the cost of less free space, x, between the devices. However, at a critical distance k, the shell provides an improvement over bare dipoles for a given free space distance, x. LHS: The arrangement of two dipoles (boxes) L_1 and L_2 with a fixed free space gap x, either with a shell (Top) or without (Bottom). RHS: Theoretical power transfer plots for these two arrangements when the shell has $R_2 = 40$ mm, $R_1 = 10$ mm.

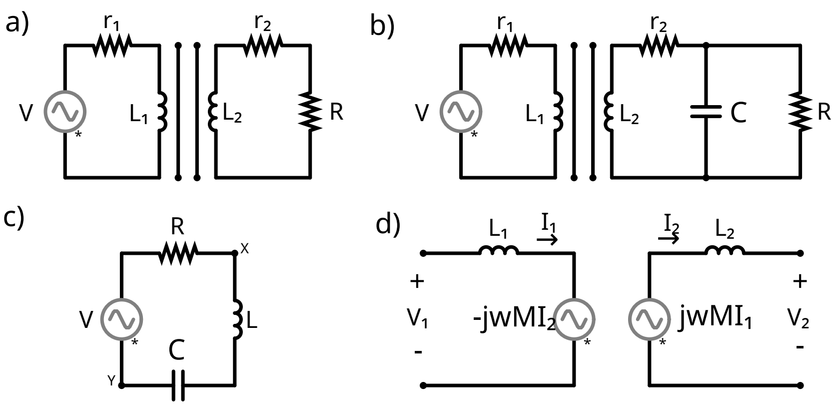

Figure 3. Wireless power transmission by inductive coupling. a) Simple circuitary for coupling L_1 and L_2 coils. The useful power transmitted is across load resistance R whilst power lost is internal resistance of coils, r_1 and r_2. b) The receiving inductor is now part of a resonant RLC circuit. c) A series RLC circuit — when voltage at x and y are in phase, the resonant condition is met. d) An equivalent circuit to the coupled inductor circuits but with explicit induced voltages shown.

and R is the ratio R_2/R_1. This arrangement and the critical distance k is shown in figure 2.

2. Methods and Circuitary

2.1. Construction of shell

0.15 mm MuMetal (MSFHP from Thorlabs) and 0.3 mm copper were cut into 21 mm by 30 mm rectangular sheets. Plastic supports for holding 36 sheets of either MuMetal or copper were 3D printed to produce the shells seen in figure 4. The inner radius R_1 and outer radius R_2 were 7 and 21 mm respectively to give an R_2/R_1 ratio of 4. The "Full shell" contains 36 sheets of alternating copper

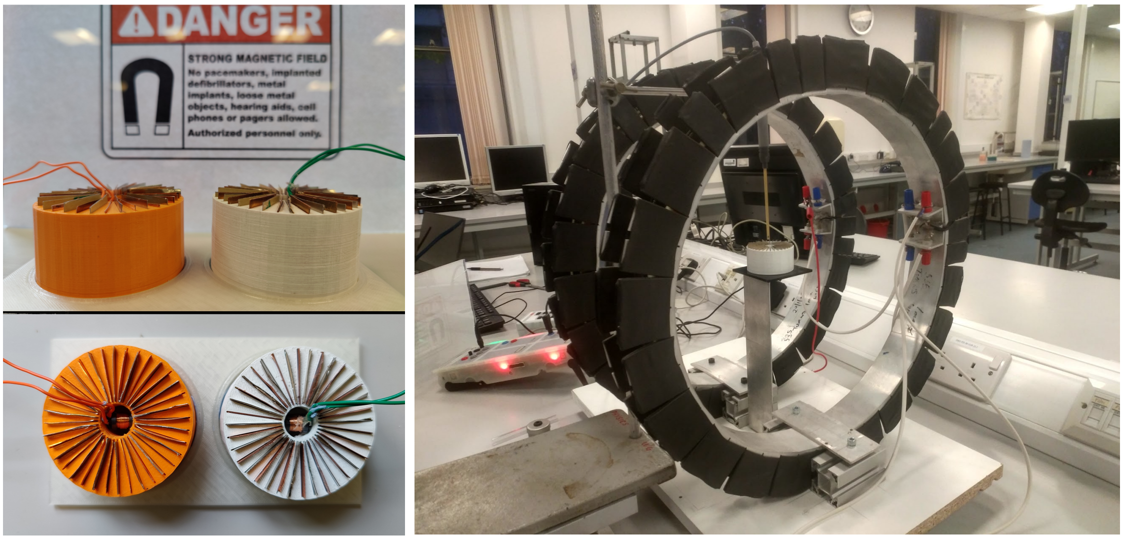

Figure 4. LHS: The constructed shells arranged in the power transfer experiment. RHS: The shell within a pair of Helmholtz coils.

and MuMetal, whilst the “No shell” scenario contains no metal.

2.2. *DC Magnetic Fields*

Helmholtz coils (figure 4) were powered by a constant DC current to create a uniform magnetic field, B, within their center described by

$$B = \frac{8}{5\sqrt{5}} \frac{\mu_0 n I}{R}, \tag{6}$$

where R is the radius of the coils, I is the current supplied to the coils, and n is the number of turns of wire. A Hall probe placed at the center of the Helmholtz coils will have a Hall voltage induced which is proportional to the magnetic field. Once calibrated the Hall probe can be used to measure the absolute value of the magnetic field present. A concentrating shell may now be placed at the center of the Helmholtz coils and the Hall probe placed within the R_1 section of the shells to explore field concentration.

2.3. *Power Transfer*

Power transfer experiments measure power dropped across a load resistor in a receiving circuit versus power lost in the transmitting circuit’s inductor. The receiving circuit, seen in figure 3, has multiple arrangements to optimise power transfer, the simplest of which is the load resistor in series with the receiving inductor forming an RL circuit. Assuming the non-ideal real resistances of the coil is $r_2 << \omega L$, then the optimal load resistance for power transfer at some frequency ω is found by,

$$V_2 = I_2(j\omega L_2 + R), \tag{7}$$

$$P_R = |I_2|^2 R = \frac{V_2^2 R}{\omega^2 L_2^2 + R^2}, \tag{8}$$

and setting $\frac{dP_R}{dR} = 0$,

$$\Rightarrow R = \omega L_2. \tag{9}$$

The EMF induced in the receiving coil of a coupled inductance system may be found by Faraday’s law,

$$\varepsilon = -\frac{d\phi_{21}}{dt}, \quad \text{or} \quad \varepsilon = -M\frac{dI_1}{dt}, \tag{10}$$

where ϕ_{21} is the magnetic flux through coil 2 due to the current of coil 1 and M is the equivalent mutual inductance between two coils. If the current in coil 1 is alternating sinuisoidally, then the maximum EMF induced in coil 2 will be $MI_1\omega$. Changes in mutual inductance for different shell constructions is a useful metric for field concentration as it is proportional to the magnetic flux present in coil 2. It may also be readily calculated if the current in coil one is known and the voltage across the load resistance in circuit 2 is measured at the optimal load resistance (equation 9). This simple relationship of voltage measurement V_2 to mutual inductance M is described by,

$$V_2 = \frac{MI_1\omega}{\sqrt{2}}. \tag{11}$$

It is well known that a resonant RLC arrangement on the receiving circuit can greatly increase the power transferred in inductive coupling[]. At resonance the complex impedance of the inductance and capacitance cancel leaving only the load resistance. Our inductance is assumed to be identical between experiments as the same coils are used and the capacitance can be found to satisfy the resonance condition at a chosen operating frequency by the relationship

$$C = \frac{1}{w^2 L}. \tag{12}$$

Practically the resonant frequency and required capacitance was found using a series RLC circuit as seen in figure 3 *c*. Resonance occurs in this circuit when V_x is in phase with V_y.
The parallel RLC PTE arrangement is considered in figure 3 *b* and may be simplified to the equivalent circuit in *d*, where the voltage across R_{load} is equal to,

$$V_2 = j\omega MI_1 - j\omega L_2 I_2, \quad \text{and} \quad I_2 = j\omega MI_1/Z_2, \tag{13}$$

where Z_2 is the total impedance of circuit 2, which in our case is a parallel RLC circuit. As with the RL case, an optimal resistance must be found to maximise power transfer. In series RLC the optimal resistance is when R_{load} matches the sum of internal resistances of the components, however in the parallel RLC case it was found that the optimal resistance depended non-trivially on the internal resistances of the components and on the frequency and inductance/capacitance values. The internal resistances of the inductance was also found to be dependent of frequency further complicating the optimal resistance calculations. The optimal resistances were therefore found experimentally through a resistance sweep at each frequency. The load voltage can then be shown to be,

$$V_2 \propto \frac{MR_{opt}}{L_2} I_1, \tag{14}$$

where R_{opt} is the optimal resistor for power transfer. All the parameters in this equation may be measured during a PTE experiment allowing the comparison of relative changes in mutual inductances (and equivalently magnetic fields) when different concentrating shells are used.

3. Results

3.1. DC Magnetic Fields

Using Helmholtz coils powered in DC to create a static external magnetic field (see Methods), we observed constant field concentration factors within the R_1 cavity for various shell constructions. No shell, 18 MuMetal, and 36 MuMetal shells were used and their concentration factor with field may be seen in figure 5*a*, where concentration factor, C, is defined as (Magnetic field within shell's cavity)/(external field produced by Helmholtz coils). It was found that the shell construction of 36 MuMetal thin sheets gave the optimum concentration factor of $C_{36} = (2.43 \pm 0.04)$ with errors likely due to the sensitivity of dipole orientation within the field. The 18 MuMetal shell gave a magnetic concentration factor of $C_{18} = (2.31 \pm 0.04)$, which suggests that the shell behaves more ideally with a greater number of sheets. Simulation work performed on COMSOL further supports this difference between 18 and 36 MuMetal sheets as shown in figure 6 *e*. The absolute values predicted by COMSOL, $C_{18} = (2.32 \pm 0.01)$ and $C_{36} = (2.46 \pm 0.02)$, closely match the experimentally observed concentration factors for both cases.

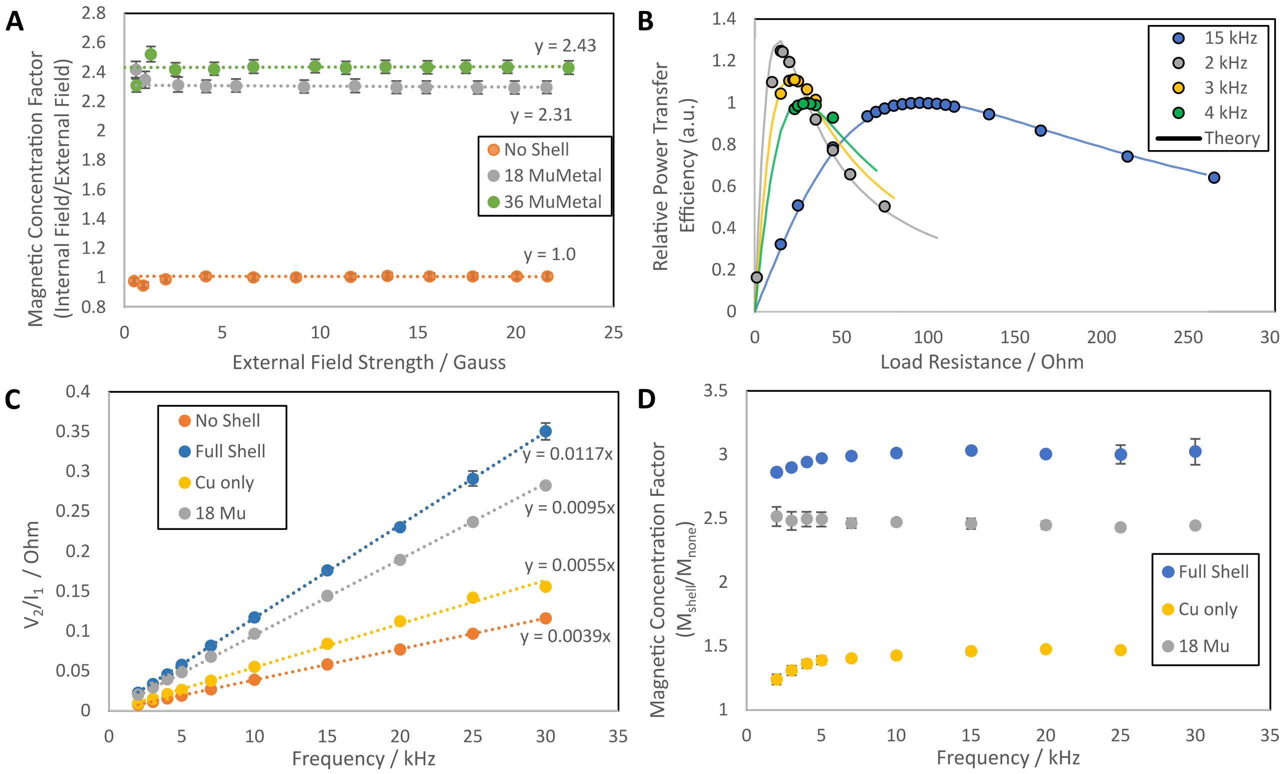

Figure 5. **A** (DC) The concentration of external static fields into the interior cavity of shells comprised of either 18 or 36 MuMetal sheets. **B** (AC) Experimentally found relative power transfer efficiencies dependence on load resistance in a coupled RL inductive circuit for various frequencies. Theory line is found using equation 9. **C** Finding mutual inductance, M, between two coils at a fixed distance for various shell configurations in the RL circuit arrangement. The gradient is equivalent to $M/\sqrt{2}$ (equation 11). **D** The shell's effect on mutual inductance is found by the ratio of (M with shell)/(M bare coil). An increase in mutual inductance corresponds to an increase in magnetic field density within the shell and is shown to be dependant on frequency for shells with copper present.

3.2. Power transfer

RL

Power is transferred from the primary circuit to a load resistor in the secondary circuit in a coupled inductive arrangement as explained in Methods. This may be simply performed by placing a load resistor in parallel with the receiving inductor L_2 forming an RL circuit as seen in figure 3 *a*. To maximise power transferred, the optimal load resistance was matched to $R = \omega L$ (see Methods equation 9). Figure 5 *b* shows the relative PTE versus load resistance for various frequencies confirming the expected optimum load resistance.

Mutual inductances between the coils at a set distance of 59 mm were found by measuring the voltage across the load resistor in the secondary RL circuit and the current driving the primary circuit and using equation 11. The copper only, MuMetal only, and full copper plus MuMetal shells all showed a concentrating effect by their relative increases in mutual inductance between the two coils as shown in figure 5 *c*. The full shell showed an increase of mutual inductance (magnetic field) by a factor of (3.0 ± 0.1), which is nearing the theoretical result from TO of $R_2/R_1 = 4$ despite only containing 36 sheets. The frequency dependance on the relative increase in mutual inductance is shown in figure 5 *d*. The two shell configurations containing copper are shown to have concentrating effects dependant on frequency. The concentrating effect rises steeply within the first 10 kHz and then plateaus for high frequencies. This expected behaviour initially motivated the choice for copper sheets in the shells for

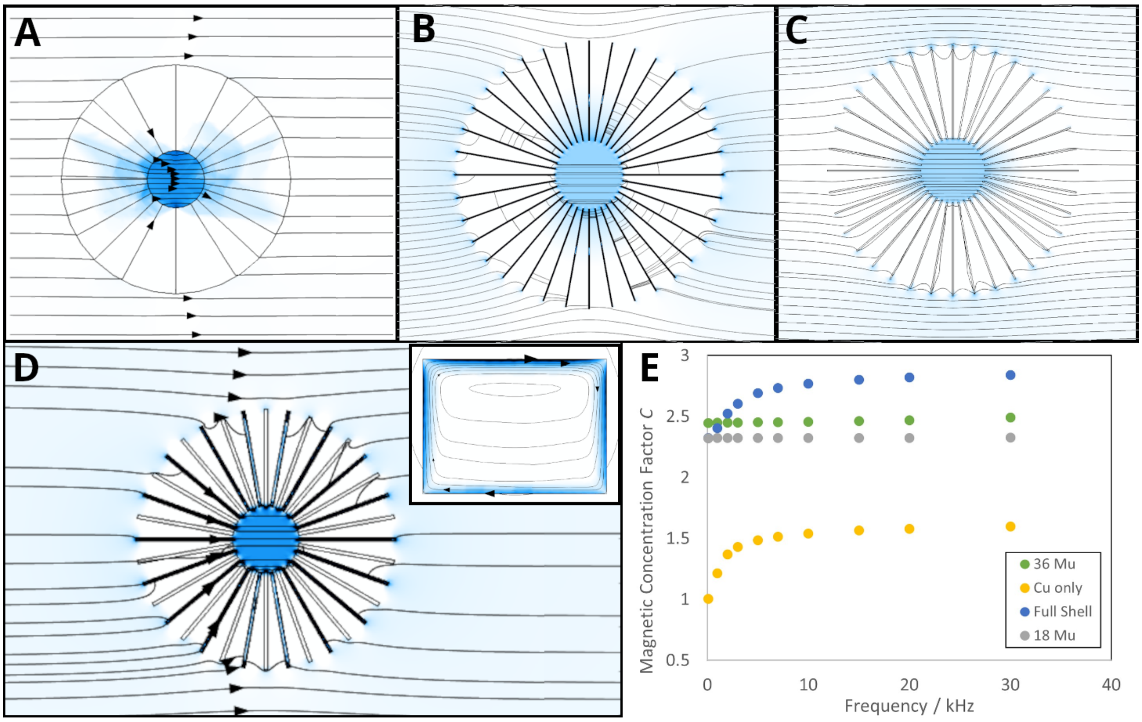

Figure 6. Exploration of magnetic field distributions using the COMSOL Multiphysics simulation package. **A)** The perfect anisotropic shell, designed by TO with infinite radial permeability and zero angular permeability, in a static external magentic field. **B)** A MuMetal only shell guiding a static field. Note the field is guided radially through the interior of the MuMetal but angular field is not adequately blocked. **C)** A copper only shell guiding an oscillating external magnetic field (30 kHz) by effectively shielding the angular component by the production of Eddy currents. **D)** A full shell comprised of alternating 18 MuMetal and 18 copper sheets in an oscillating external magnetic field (20 kHz). The dimensions of the simulated shell matches those of the real fabricated shells. The MuMetal sheets are darker due to guiding the field within their interior whilst the copper sheets deflect's the angular component of the fields. The inset image is the Eddy current density within a single copper sheet with a perpendicular applied magnetic field. **E)** The dependence of magnetic concentration of various shells on frequency of the oscillating field. It can be seen that the two shells with copper show improved concentration as frequency is increased as predicted and also shown experimentally.

AC power transfer. At higher frequencies the perpendicular component of alternating magnetic fields produce eddy currents within the copper which, due to Lenz's law, oppose the change of field direction and effectively increases the angular permeability of the shell. Supporting work done on COMSOL (figure 6 $b - e$) shows a similar observed effect where 36 copper sheets increases the concentration factor rapidly from $C = 1$ at 0 Hz to $C \approx 1.5$ by 10 kHz and then only a small further increase in efficacy at higher frequencies.
Apart from errors due to instrument, measurement reading, and coil placement, we observed noise due to stray magnetic fields inducing pick-up within cables connecting the solenoid to the lock-in amplifier. This source of noise is highly frequency dependent and is at the same frequency as our desired signal, so could not be removed by the use of a lock-in amplifier. To supress this noise careful cable placement and shielding was installed.

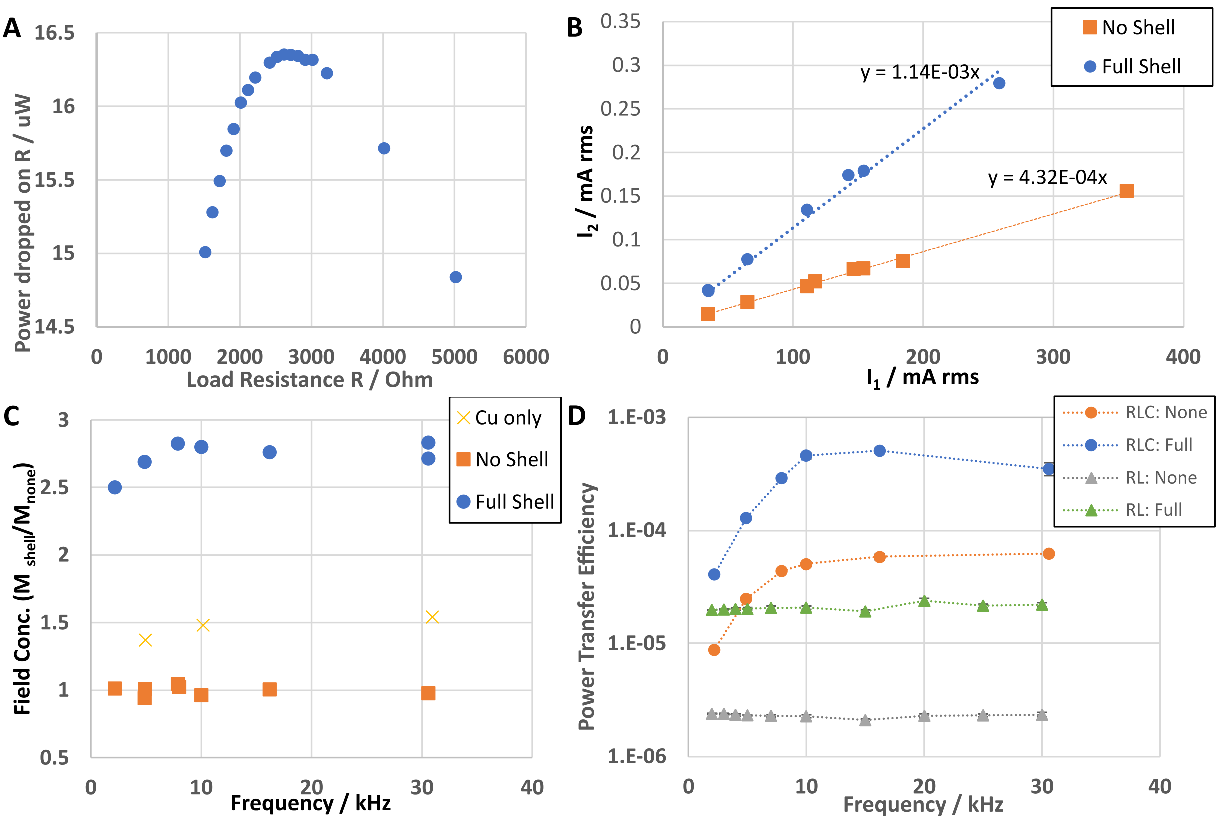

Figure 7. A) Locating the optimal load resistance for power transfer in a parallel RLC receiving circuit at an AC frequency of 30 kHz. **B)** The current across the optimal load resistor is proportional to mutual inductance in the resonant parallel RLC circuit. Comparing the gradients of I_2 against I_1 for the case when a shell is present to when one is not presents gives the factor increase of mutual inductance which is equivalent to the concentration of the field within the shell. **C)** The shell's effect on mutual inductance in an RLC circuit is found by the ratio of (M with shell)/(M bare coil). As with the RL circuit, the concentration of field is dependant on frequency for the full shell which has copper present. **D)** A comparison of power transfer efficiencies (PTE) for both a full shell (18 copper and 18 MuMetal sheet) and no shell in either the RL and RLC case. PTE is given as a ratio of power dropped across the load resistor against power lost in the transmitting coil as explained in Methods.

Resonant — RLC

Parallel RLC circuits are more fitting for optimising power transfer [?] as explained in Methods. For the arrangement described in figure 3 *b*, a full shell comprised of 18 MuMetal and 18 copper sheets was explored. The optimal load resistances were found experimentally by measuring power for a sweep of resistances, an example of which is shown in figure 7 *a* for a field frequency of 30 kHz.
From equation 14 the voltage measured across the load resistor is proportional to the mutual inductance between the two coils when the optimal load resistor is used and the resonance condition for the RLC circuit is met. Figure 7 *b* confirms this relationship and shows an increase of mutual inductance when the full concentrating shell is present. The gradient was found to be increased by a factor of (2.6 ± 0.2) corresponding to a field concentration of the same factor if the inductance of L_2 is assumed to remain constant.
The frequency dependance on concentration factor is shown in figure 7 *c* and it can be seen that, as with the RL and simulated experiments, the presence of copper in the shell leads to a low initial

concentration which increases with frequency until around 10 kHz at which point the concentration factor plateaus.
The PTE for RL and RLC, no shell and full shell arrangements are compared in figure 7 *d*. It can be seen that the shell increases the efficiency in both cases by a similar factor and that the parallel resonant RLC arrangement gives a much greater efficiency than using the simpler RL circuitary.

4. Discussion

For the constructed shells used in these experiments, their R_2/R_1 ratio was (4.0 ± 0.2) and from the theoretical TO work, it was predicted that the field should be concentrated in the perfect shell by the same ratio. The greatest concentration of field we observed was $C_{Full} = (3.0 \pm 0.1)$ in the AC RL case. This concentration is still well below the expected theoretical concentration factor of $C = (4.0 \pm 0.2)$ and likely explained by our approach to approximating the perfect TO designed anisotropic shell to a discretized version comprised of sections of high and low permeability. In both static and oscillating fields, experimentally and in simulations, we found that 36 MuMetal sheets performed better than 18 MuMetal sheets which suggests that finer discretization of the proposed shells gives concentrations closer to the theoretical value. Furthermore, in the static field experiments, only air was used to approximate the zero relative angular permeability. Air has a permeability of $\mu_r \approx 1$, which although is far less than the MuMetal's $\mu_r = 55,000 - 75,000$, is likely still a poor approximation. This can be seen by the increase in performance in the oscillating external field experiments where copper sheets are introduced in order to effectively screen out angular field density by the production of Eddy currents.
Previous work by Pratt et. al.[] included the exploration of MuMetal and superconducting shells for concentrating static magnetic fields. This work quoted a concentration factor of XXX at T¡Tc and XXX at T¿Tc.

We assumed the inductance of the solenoid was independent of the shell surrounding it. Here we shall reexplore some results without this assumption.
The resonant condition of a series RLC circuit (figure 3 *c*) allows the calculation of effective inductance L using the known capacitance and found resonance frequency. The inductance of the bare coil or when surrounded by a copper only shell was (1.02 ± 0.02) mH whilst the coil surrounded by the full shell was found to be (1.25 ± 0.01) mH. This increase in inductance can be understood by the high permeability MuMetal in the shell being located near to the coil, which increases the relative permeability of space in the vicinity of the coil. A change in inductance will effect the power transfer efficiency as described by XXX equation **??**. The use of a resonant parallel RLC setup within the receiving circuit can counteract this loss of power transfer as the optimum load resistance in this case does not depend as strongly on the inductance value, but rather on internal resistances of the components.

Due to the sharp drop off of power transfer with distance, the greatest PTE found was 1.01% XeX at a seperation of 48.7 mm with both the transmitting and receiving coil surrounded by a concentrating shell. The reason for this poor efficiency is largely due to the non-ideal real resistive component of the transmitting coil...

DC:
- further explanation on error source in placement

Power transfer
- Generally low PTE due to high loss of inductor. Could have used laminated AC inductor to reduce eddie currents. Could have not used iron core as hysteresis.
- Discussion of other power transfer techniques and coupled inductor papers. Why a shell is better than no shell with distances.

- Why a shell allows a small radii inductor to be used - efficiency of scale Better coupling for given distance. See p.51 pratt.
- Relationship of PTE with distance -$r^{-5.6}$. Effective mutual inductance changed.
- Two shells present.
- Another exploration on error sources and summary of largest sources.

Comparison of RL, series RLC and parallel RLC circuitary:
- models
- expected efficiency

5. Conclusions

EXTENSIONS
0) For further understanding we would need to look at more frequencies and expecially at much higher freqs. A selection of different dipoles would also be beneficial to ensure that frequency dependence is not linked to non-ideal dipole.

0) Perhaps another circuit could be designed that works more similarly to an RLC? Could propose one however experimentation has not been performed.

0) Could a more complicated and directional shell be designed for power transfer?

6. References